On-line Quantification of Thickness and Strength of Single and Mixed Species Biofilm Grown Under Controlled Laminar Flow Conditions

Oliver P. W. Peck, Y. M. John Chew* & Michael R. Bird

Centre for Advanced Separations and Engineering, Department of Chemical Engineering, University of Bath, Claverton Down, Bath BA2 7AY, UK

*corresponding author: y.m.chew@bath.ac.uk

Abstract

This study describes cleaning investigations of biofilms comprised of *Escherichia coli* and *Burkholderia cepacia* grown on polyethylene, stainless steel and glass substrates. Their adherence behaviour was determined under controlled hydrodynamic conditions using the non-contact technique of Fluid Dynamic Gauging (FDG). FDG utilises flow data to estimate (i) the adhesive (between biofilm and substrate)/cohesive (between cells and extracellular polymeric substances) strengths, and (ii) the thicknesses of biofilms. The thickness of single and mixed species biofilms increased linearly with time and plateaued at 14 days with no significant reduction thereafter. The asymptotic thickness of mixed species biofilm were thinner than *E. coli* biofilms. The adhesive strength, on the other hand, peaked at approximately 14 days with a significant reduction thereafter. The results showed that the development of biofilm thickness and attachment strength are not affected by the range of surface roughness and surface energy employed. However, the increase in strength is strongly correlated to the protein and glucose content of the biofilms. Confocal laser scanning microscopy results confirmed an increase in the percentage of dead cells after 21 days, contributing to the weakening of the biofilms. Interrupting the flow of media during biofilm development had a negligible impact upon the thickness, but was found to significantly increase the biofilm strength.

Keywords

Biofilms; Drip-flow; Strength; Thickness; *Escherichia coli*; *Burkholderia cepacia*

1. Introduction

Biofouling is ubiquitous in a number of fields including food and pharmaceutical production, shipping, steel manufacturing, petrochemicals, water desalination, and drinking water treatment and distribution. Biofilms can grow on all surfaces that are exposed to local bacteria inhabitation such as pipe bends, conveyor belts, floors and rubber seals. Biofilms consist primarily of viable and nonviable embedded in polyanionic extracellular polymeric substances anchored to a surface (Carpentier and Corf, 1993). The initial microorganism attachment is reversible, and may be the rate limiting step of the entire growth process. The bond with the surface is consolidated when irreversible attachment begins to take place, which is initiated by the production of extracellular polymeric substances (EPS) (Whitehead and Verran, 2015; Garnett and Matthews, 2012; Yebra *et al.*, 2006; Momba *et al.*, 2000). EPS are produced and excreted by the micro-organisms of interest, with a chemical structure dependent upon both the species involved and the environmental conditions. They may contain polysaccharides, proteins, phospholipids, teichoic and nucleic acids, and other polymeric substances hydrated to 85 to 95% water. The EPS is responsible for most of the characteristics of the biofilm, ranging from structural benefits, such as instigating the adherence of biofilms to surfaces and the formation of a gel-like network keeping the bacteria together, to the protection of bacteria against potentially damaging influences from the environment. Arguably the most important function of EPS is their role as fundamental structural elements determining the mechanical stability of biofilms (Wingender *et al.*, 1999).

The disinfection of biofilms is a problematic task due to the range of defence mechanisms they possess. The threat of biofouling cannot be entirely eliminated as antifouling measures are only temporary or time-dependent restrictions of growth, and regular disinfection is therefore required in order to prevent their continuous development (Flemming *et al.*, 2011). Current pre-treatment technologies focus on the reduction in microorganisms in the feed source, which may not provide effective biofouling control since biofilm development relies heavily on the surface chemistry of

substrates and availability of nutrients (Chen *et al.*, 2013; Jamaly *et al.* 2014). Chemical agents are often employed to kill microorganisms, but the biofilm structure must be removed to prevent re-growth and maintain sterility. The required concentration of antibacterial agents is also considerably higher, and must be increased by between 10 and 100 times in comparison with the respective equivalent planktonic cultures (Blanchard *et al.*, 1998). To avoid the use of chemical agents that can pose health and environmental risks, the usual methods of biofilm deactivation involve pumping large volumes of cleaning solutions through pipelines to achieve the additional benefits of mechanical cleaning.

There are numerous of studies and review articles related to biofilm formation and characterisation of their properties, and mitigation of biofouling (e.g. Bucs *et al.*, 2018; Wang and Lan, 2018; Gule *et al.*, 2016; Srey *et al.*, 2013). In general, these studies can be grouped into three main areas: biofilm surface characteristics, biofilm structure and thickness, and biofilm adhesion to a surface. A variety of lab-based on-line methods for estimating the thickness and development of biofouling have been explored and reported. These methods include microscopic (e.g. confocal laser scanning microscopy) (Mukherjee *et al.*, 2016), spectroscopic (e.g. infrared, nuclear magnetic resonance and Raman spectroscopy) (Kögler *et al.*, 2016) and ultrasonic time-domain reflectometry (Sim *et al.*, 2013). Atomic force microscopy (AFM) is probably the only technique that allows the measurement of the physical adhesive forces of foulants to surfaces in situ, which may include bacterial and biofilm adhesion to surfaces (Powell *et al.*, 2017). However, it is especially challenging to obtain reliable measurements in flow systems commonly employed in industry.

Previous studies from the authors have focused on single species biofouling and cleaning experiments by using static culture (Peck *et al.*, 2015) and turbulent duct-flow (Suwarno *et al.*, 2017) systems. The main aim of this study was to seek more sustainable methods of effective biofilm deactivation and removal whilst reducing chemical, water and energy consumption. This work presents

experiments of single and mixed species cultures of *Escherichia coli* Nissle1917 and *Burkholderia cepacia* biofilms grown on polyethylene, glass and stainless steel 304 under controlled laminar flow conditions in a modified drip flow reactor. M9 minimal medium containing glucose was used to provide an artificially designed source of minimum nutrients for growth. The technique of fluid dynamic gauging (FDG) was utilised to quantify both the thickness and the strength of the biofilms incubated for up to 28 days *in situ*. This study also explored the effect of biofilm content and the impact of desiccation which could occur due to flow disturbances or during cleaning (*i.e.* transition from feed to cleaning formulations) on growth and removal.

2. Materials and methods

2.1 Bacteria strains, culture media and substrates

Escherichia coli Nissle1917 and *Burkholderia cepacia* DSM-7288 were used to grow single species and mixed biofilms under controlled laminar flow conditions. *E. coli* is recognised to form biofilms on many different surfaces, which is essential for the studying and comparison of fouling mechanisms with an industrial focus. Protocols for *E. coli* biofilm growth are well-established and it has been extensively characterised. *B. cepacia* was selected as an additional species for mixed species biofilm development. Interest in its occurrence in industrial scenarios is emerging, due to its ability to survive prolonged exposure to high concentrations of many common industrial biocides, including benzalkonium chloride and triclosan (Rose *et al.* 2009).

The medium used in this study was M9 minimal medium (De Kievit *et al.*, 2001), containing 47.7 mM $Na_2HPO_4.7H_2O$, 21.7 mM KH_2PO_4, 8.6 mM NaCl, 18.7 mM NH_4Cl, 0.5% (wt/vol) Casamino acids, 1 mM $MgSO_4$ and 11.1mM glucose (all sourced from *Sigma Aldrich*).

Three different substrates were used: (i) polyethylene (PE), (ii) glass, and (iii) stainless steel 304 (SS). Each surface was fabricated into small strips with dimensions of 60 mm (length) × 25 mm (width) ×

1 mm (depth). For fouling and cleaning tests, each test surface was made up from three small strips of different surfaces to give a total length of 180 mm. This was to maximise the number of biofilm samples per experiment. Prior to each growth experiment, the surfaces were washed with isopropanol solution.

The proliferation, size and shape of surface imperfections are known to be a factor in the process of microorganism adhesion and therefore also in biofilm establishment. The properties of each surface were characterised using atomic force microscopy (AFM) and contact angle analysis. The surfaces were examined using AFM in order to visualise the morphological profiles in high resolution. A Digital Instruments Nanoscope IIIA (with a tip length of 225 μm) was operated in the tapping mode and the size of the scanned surface used was 5 μm × 5 μm. Along with the roughness of surfaces, surface energy (and therefore wetting potential) is also widely recognised to play a role in the propensity of biofilms to attach to various surfaces (Finlay *et al.*, 2002). A set of critical surface tension tests were therefore conducted by using the Zisman plot method. This method was selected due being relatively quick and simple to conduct, whilst being recognised to be accurate. Here, measurements were compiled using water and 5, 10, and 15 wt% NaCl test solutions. Contact angle measurements were carried out using a Dataphysics Contact Angle System OCA. Three measurements were taken for each NaCl concentration on each surface in order to attain repeatability.

2.2 Apparatus and growth conditions

The experimental set-up is shown in Figure 1. The M9 minimum media with glucose was stirred with an overhead mixer in a 30 L tank and maintained at a temperature of 37ºC by using a water bath (Figure 1(a)). The bacteria stock solution (cell counts ~ 10^6 CFU ml^{-1}) was injected at a rate of 0.25 ml min^{-1} using an injection pump (ELDEX, model 5979-Optos Pump 2HM). The details of preparation of the bacteria stock solution has been reported in Peck *et al.* (2015). Briefly, the species were cultured overnight at 37ºC, diluted in fresh media to an optical density (OD600) of 0.06. 200

µL of each diluted culture was added to wells of a 48-well polystyrene microtitre plate, with four plates dedicated to each strain plus another row of pure medium for control purposes. The microtitre plate was then placed on an incubator (Stuart Mini Gyro-Rocker SSM3) at 37°C, rotating at maximum speed of 70 rpm. After 24 h the supernatant fluid was pipetted out and replaced with another 200 µL of fresh medium. Incubation was resumed for another 24 h period. The absorbance of the content of each well (including the control wells) were measured and recorded using an automatic plate reader (VERSAmaxTunable Plate Reader BN 02877) at a wavelength of 595 nm, as wavelengths in the region of 600 nm are a good option for most bacterial cultures, with the advantage that the media components contribute less to the overall absorbance than at lower frequencies (Burton and Kaguni, 1997). The medium and bacteria stock was flowed into the drip flow reactor (Figures 1(b) and (c)) by gravitational effect at a constant rate of 1.0 L h^{-1}, which gave a Reynolds number of ~ 15 in the flow cell, for durations of 5, 10, 14, 21 and 28 days. The effluent from the reactor was then drained. The feed tank was topped up with fresh media every 24 h. The bacterial stock solution was replenished within every 24 h to further ensure a controlled feed condition throughout the whole experiment duration. For mixed species biofilms, approximately equal, half volumes of both organisms (~ 0.5 × 10^6 CFU ml^{-1}) were used for inoculation. All experiments were repeated twice except for 21 and 28 days where only one repeat was carried out. Statistical analyses were performed using Student's *t*-test. Measurements were considered significantly different when a *p*-value was less than 0.05.

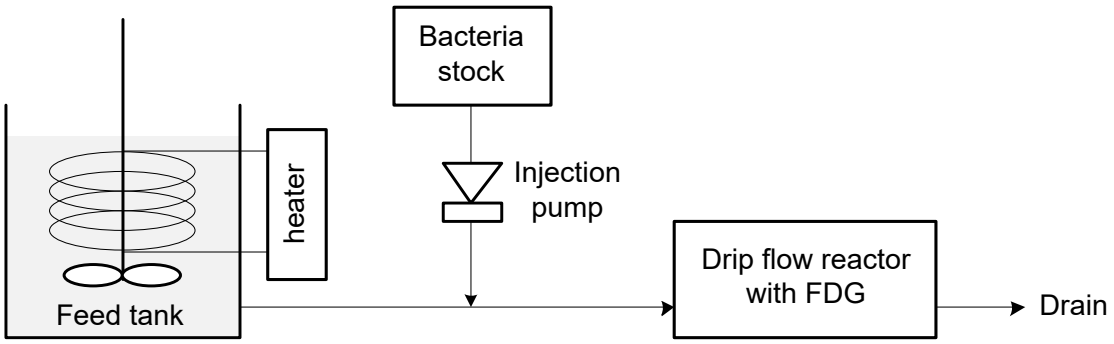

(a)

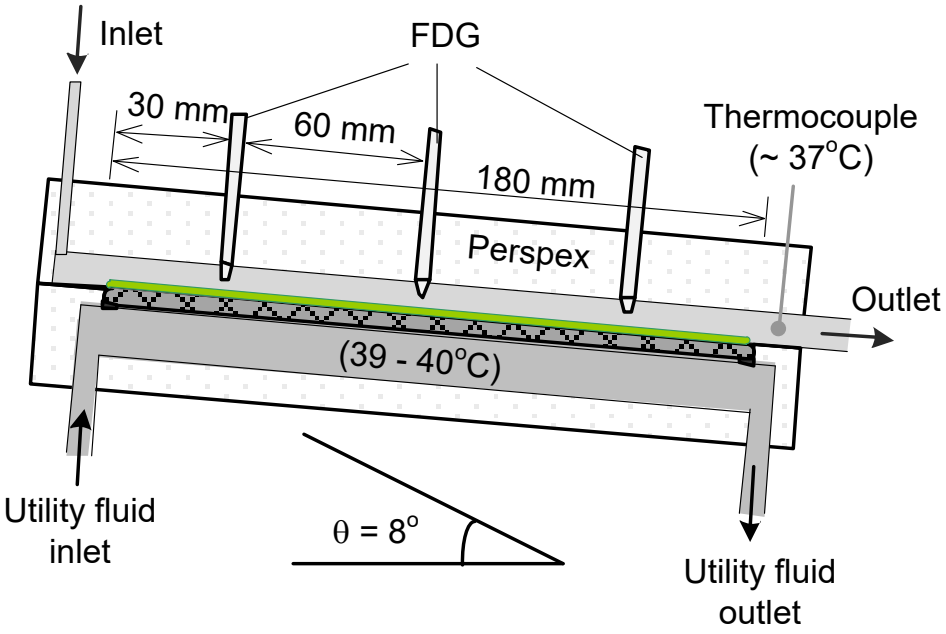

(b)

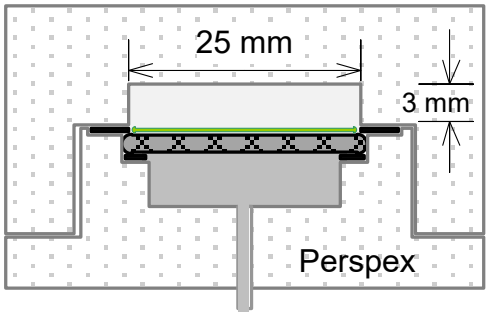

(c)

Figure 1: Schematic representation of the (a) flow apparatus for biofouling experiments, (b) drip flow reactor with *in situ* measurements from fluid dynamic gauging at three locations, and (c) the cross section of the test channel.

The technique of FDG testing (Figure 2) was conducted on-line (under the same operating conditions) at the end of every biofouling experiment. The experiments were identified as 5-day, 10-day, 14-day, 21-day and 28-day. The details of the application of FDG to measuring the thickness and strength of biofilms have been reported in Peck *et al.* (2015) and Suwarno *et al.* (2017). All FDG testing was carried out at a constant gauging flow rate, m_g, of 0.2 g s^{-1}. The thicknesses of biofilms were estimated by comparing the pressure drop measurements across the nozzle against a calibration profile pre-

determined using a clean substrate. The strengths of the biofilms were calculated by using equation (1) *i.e.* an analytical approximation of flow between parallel discs (Chew *et al.*, 2004):

$$\tau_w = \frac{6\mu m_g}{\rho\pi h^2}\frac{1}{d_t} \qquad (1)$$

where τ_w is the shear stress exerted by gauging flows, ρ is the density of the liquid, μ is the dynamic viscosity of the liquid and h is the clearance between the nozzle and the biofilm.

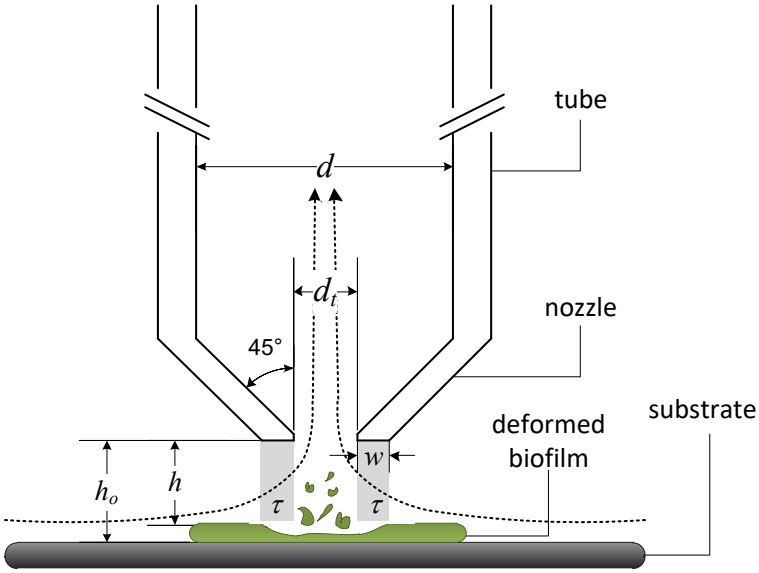

Figure 2: Principles of FDG and the shaded region underneath the nozzle indicates the shear stress exerted by gauging (suction) flows that cause biofilm removal. Nozzle dimension: d = 2 mm, d_t = 0.5 mm and w = 0.25 mm.

Apart from the biofouling experiment at varying durations, an additional experiment was conducted by performing a 5-day biofouling experiment, followed by 24 h desiccation under no duct flow and no nutrient supply, followed by another 5-day biofouling experiment. This experiment was aimed at investigating the impact of flow cessation due to possible process interruption in industrial processes. This experiment is identified as 10*-day.

2.3 Confocal laser scanning microscopy

Confocal laser scanning microscopy (CLSM, *Zeiss* CLSM 510META) images of stained *E. coli* biofilms on glass surfaces were taken to identify the presence of living and dead cells. The tendency of cells to die or lyse at a particular stage of their life span has been linked to biofilm dispersal (Schleheck *et al.*, 2009), and dual staining can be conducted in order to clearly depict regions of dead cells. A combined stock solution of fluorescent dyes 1mM acridine orange and 1mM propidium iodide in phosphate-buffered saline (PBS with a composition of 8 g L^{-1} NaCl, 0.2 g L^{-1} KCl, 1.15 g L^{-1} $Na_2HPO_4.7H_2O$ and 0.2 g L^{-1} KH_2PO_4, pH adjusted to 7.3) was made for staining (Mascotti *et al.*, 2000). Acridine orange binds to nucleic acids, which allows it to produce a green fluorescence from live cells present. Propidium iodide, on the other hand, enters cells with compromised membranes, staining dead cells red. The samples were covered with foil when left to stain, as acridine orange is vulnerable to degradation under direct sunlight.

2.4 Protein and polysaccharide quantification in EPS

The nature of EPS composition of biofilms was investigated, and in doing so trends may be revealed which relate to changes in thickness and strength of attachment. The protein and polysaccharide levels were characterised using the cation exchange method. At the FDG testing, the biofilm was removed from the surface with a cell scraper and suspended in PBS and shaken for 30 minutes. The sample was then placed in an ultrasonic bath for 2 minutes followed by homogenisation with an ultrasonic probe in pulsating mode for 10 pulses at 45 W. This treatment has been shown to be effective for cell removal (Dreszer *et al.*, 2013), ensuring that the EPS can be analysed in isolation. Finally, the EPS was dissolved into the liquid. This was achieved via the addition of a cation exchange resin in the sodium form (Na^+) at a rate of 0.2 g per 1 mL sample. The mixture was shaken for 2 h at room temperature. The Na^+ in the resin was exchanged for the Ca^{2+} in the sample, allowing for the dissolution of the EPS. The suspension was then centrifuged for 20 minutes at 4ºC to separate the cells from the EPS for effective content analysis.

The procedure for protein quantification using bicinchoninic acid (BCA) was described by Smith *et al.* (1985). The standard BCA reagent consists of two components. Reagent A was a solution containing 1% BCA-Na_2, 2% $Na_2CO_3.H_2O$, 0.16% Na_2 tartrate, 0.4% NaOH and 0.95% $NaHCO_3$. Reagent B was 4% $CuSO_4.5H_2O$ in deionised water. The standard working reagent (SWR) was formed by mixing reagents A and B to the ratio of 50:1. The quantification procedure began by mixing 100 µL of sample (standard or test) with 2 mL of SWR in a test tube. Immediately, a colour change was observed. The absorbance of the samples was then measured at 562 nm and compared to a reagent blank. This allows a standard curve to be plotted, or for a test sample to be compared to a previously compiled standard. In this instance, bovine serum albumin was used as the protein standard for comparison.

A similar method for polysaccharide quantification was described by DuBois *et al.* (1956). The two reagents required in this case were grade 95.5% sulphuric acid and 80 wt% phenol solution (prepared by adding 20 g of glass distilled water to 80 g of redistilled reagent grade phenol). 2 mL of the standard (glucose in this case) or test solution was pipetted into a test tube, followed by 0.05 mL of the phenol solution. Subsequently, 3 mL of sulphuric acid was added rapidly. They were then left to stand for 10 minutes, and then heated in a water bath at 25^{o}C for a further 10-20 minutes. Absorbance was measured at 490 nm.

3. Results and discussions

3.1 Surface roughness and energy

Table 1 shows the roughness of polyethylene, stainless and glass substrates determined by using AFM in tapping mode. All surfaces appear to be relatively smooth and exhibit similar roughness profiles. These irregularities are significantly lower in comparison to the size of the cells (both species are typically approximately 2 µm in length) and would offer nothing in the way of shelter or enhance

surface area for colonisation. Therefore, it seems unlikely that surface roughness will play an important role in any distinctions between the surfaces employed in this study. From Table 2, it can be taken that the glass substrate is the most hydrophilic, followed by stainless steel, with polyethylene being the most hydrophobic. In general, though, hydrophobic surfaces are considered to promote more adhesion, although there has been conflicting research on this. Alsteens *et al.* (2007) reported that hydrophobic surfaces generally promote cell adhesion in conjunction with protein folding and aggregation, and that they are favoured by all bacteria. Other research (e.g. Bos *et al.*, 2000) has showed that hydrophobicity plays a greater role in biofilm retention than in the additional adhesion. In this work, the effect of surface hydrophobicity showed little effect on the biofilm thickness and strength data (shown in later sections). This is similar to the results observed by Gilbert *et al.* (1991) and Carpentier and Cerf (1993) where they showed the adhesiveness of *E. coli* on stainless steel is not influenced by hydrophobicity. Further analysis of cell-surface interactions such as AFM (not performed in this study) will be required to confirm this observation.

Table 1: The average roughness, R_a, root mean square roughness, R_{rms}, and average peak-to-valley height, R_z, of polyethylene, stainless and glass substrates.

	Polyethylene	**Stainless steel**	**Glass**
Average roughness, R_a [μm]	0.26 ± 0.02	0.21 ± 0.03	0.18 ± 0.02
Root mean square roughness, R_{rms} [μm]	0.32 ± 0.04	0.27 ± 0.03	0.24 ± 0.04
Average peak to valley height, R_z [μm]	0.82 ± 0.08	0.74 ± 0.08	0.83 ± 0.06

Table 2: Air-liquid surface tension of different test liquids (from standards), and contact angle measurements and critical surface tension (**BOLD**) of polyethylene, stainless and glass substrates.

Test liquid	**Air-liquid surface tension** [mN m^{-1}]	**Polyethylene** cos θ	**Stainless steel** cos θ	**Glass** cos θ
Water	72.7	0.18 ± 0.03	0.78 ± 0.03	0.83 ± 0.01
5 wt% NaCl	74.4	0.12 ± 0.02	0.70 ± 0.02	0.80 ± 0.01
10 wt% NaCl	76.2	0.07 ± 0.01	0.68 ± 0.02	0.67 ± 0.03
15 wt% NaCl	77.9	0.02 ± 0.01	0.59 ± 0.02	0.52 ± 0.02
Critical surface tension [mN m^{-1}]	**-**	**46 ± 2**	**66 ± 2**	**70 ± 2**

3.2 Growth curve

Both the *E. coli* and *B. cepacia* strains were grown in suspended liquid culture in M9 media with glucose, with the optical density (OD600) being recorded after each hour (Figure 3). This was continued up to the point at which there ceased to be an increase in optical density and a stationary phase was reached. It should be noted that dead cells were not differentiated by this analysis, so no meaningful decrease of viable cells were recorded. Scanning electron micrographs of mono-cultured *B. cepacia* and *E. coli* cells showed very similar dimensions *ca.* 0.5 μm (width) × 2 μm (length) (Peck, 2017). It is not straightforward to differentiate the cells under SEM. Bacterial identification technique such as ribotyping (Schumann and Pukall, 2013) is one possible way of differentiating the species. This is, however, not carried out in this work.

The growth curve for *E. coli* shows the initial lag phase in which there is a delayed growth in cell numbers, followed by the exponential growth phase between 2 and 6 h where multiplication of cells accelerates rapidly. There is also clear evidence that the culture entered its stationary phase after about

6 h. It was not possible to observe any death of mature cells using this particular method. The growth curve for *B. cepacia* displays the same core characteristics as *E. coli*'s. The initial lag period, followed by the phase of exponential growth and finally the stationary phase are all distinctly noticeable. However, it can be seen that the lag phase is more prolonged, taking at least 3 h before growth begins to escalate. A stable maximum level is only reached after 9 h, which is a considerable delay in comparison with the *E. coli* growth curve. It should be noted that bacteria from biofilms show different physiological properties in their response to environmental influences compared with bacteria growing planktonically. The growth rate of bacteria in the biofilm is generally slower than in the planktonic phase due to the restricted availability of nutrients (Wimpenny *et al.*, 1993). The amount of nutrients diffusing from adjacent environment into the biofilm diminishes and as the biofilm grow thicker the diffusion of nutrients and oxygen is also hampered.

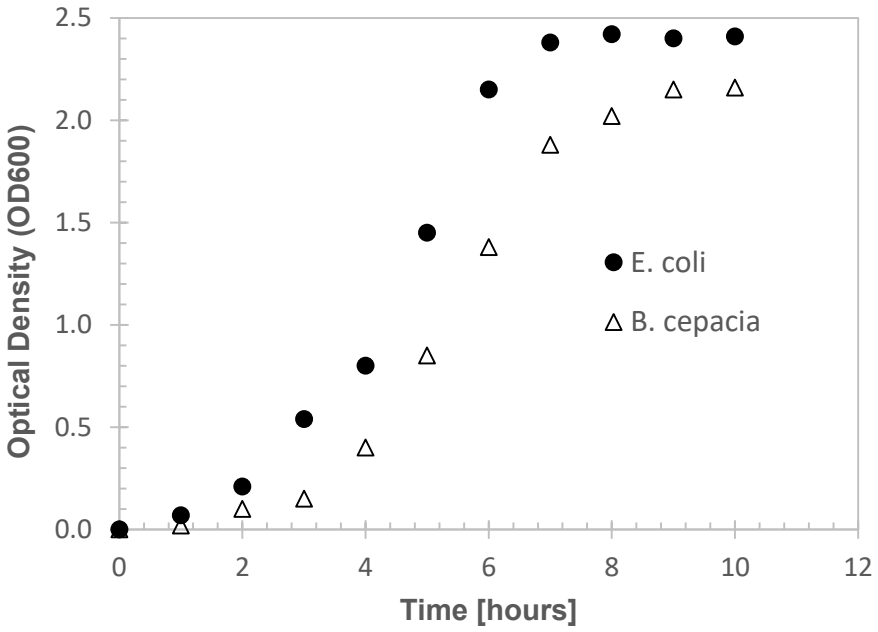

Figure 3: Growth curve of individual *E. coli* and *B. cepacia* strains in suspended M9 mimimum media with glucose.

3.3 Biofilm thickness

Biofouling experiments were conducted for durations of 5, 10, 14, 21 and 28 days, and FDG analysis was conducted at the end of every experiment. Typical biofilm thickness measurements are shown in Figure 4. The average thickness of both the *E. coli* and mixed species biofilms increased rapidly from 5 days through to 14 days, after which time the thickness reached a plateau. An interesting observation is that the growth rate for both types of biofilms was similar for up to 14 days duration. Beyond 14 days the presence of *B. cepacia* in the mixed species biofilm caused an apparent thinning of the asymptotic thickness by approximately 30 μm. The thinning of mixed species biofilm was similar to that reported by Makovcova *et al.* (2017) where they observed thinner mixed biofilms formed by *E. coli* and *Staphylococcus aureus*. It is also noteworthy that the effect of the 24 h desiccation protocol upon the thickness of 10-day biofilms was found to be insignificant.

Table 3 summarises the statistical analysis on the thickness measurements for both *E. coli* mono-culture and mixed species biofilms. Measurements were considered significantly different when a *p*-value was less than 0.05. The results confirm that the roughness and hydrophobicity of the different surfaces did not significantly affect the biofilm thickness, apart from once case - PE vs Glass, 5-day.

Figure 5 suggests that the concentrations of protein and polysaccharides in a biofilm do not increase in direct proportion to the thickness of the biofilm. Both figures show that the thickness of the biofilms continue to increase whilst the protein and glucose levels peak at around 10-14 days and 10 days, respectively. The key difference is that the thickness does not experience a decline as the incubation period is extended towards the later ages. This could signify either a decrease in biofilm density or a degradation of EPS even as the cells continue to reproduce. It may coincide with the phase of dispersal, where it is considered easier for the outer layers to slough off with low resistance.

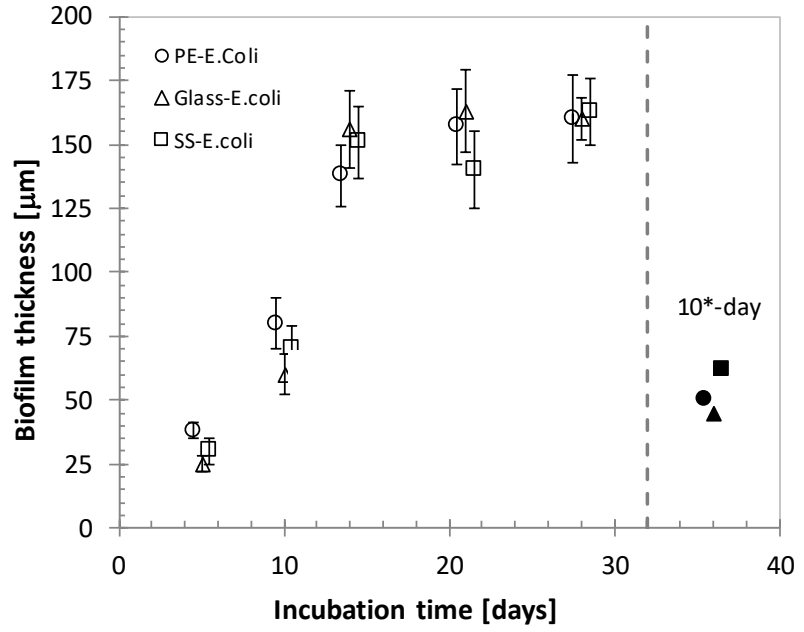

(a)

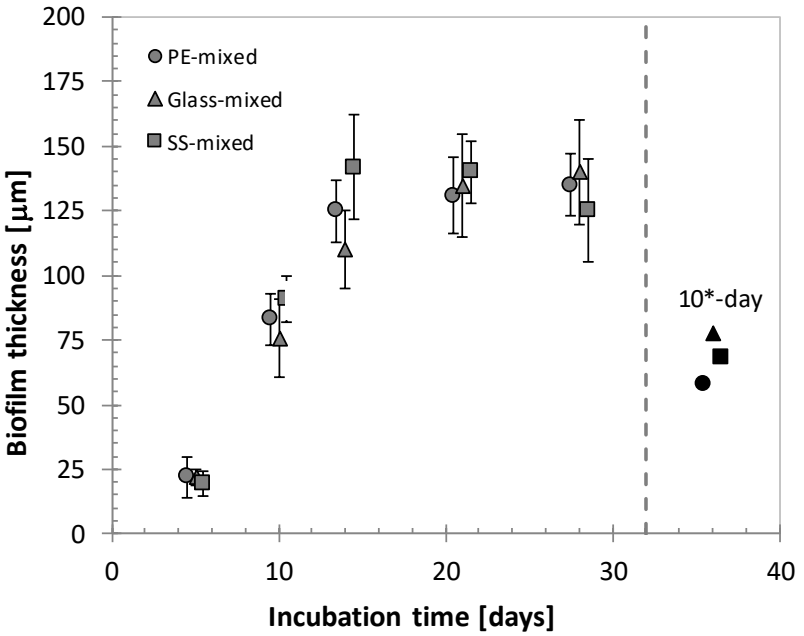

(b)

Figure 4: The average thickness of (a) *E. coli* and (b) mixed species biofilms grown under constant flow conditions as measured by FDG. The error bars show the minimum and maximum thicknesses measured for each incubation period. 10*-day indicates biofilms grown for a total of 10 days with dessication on day 5 for 24 h.

Table 3: Student's *t*-test of thickness measurements of *E. coli* and mixed species biofilms presented in Figures 4(a) and (b). Measurements were considered significantly different when a *p*-value was less than 0.05. (n.s.: no significant difference *i.e.* $p > 0.05$)

Days	PE vs Glass	Glass vs SS	SS vs PE
		E. coli	
5-day	$p < 0.01$	n.s.	n.s.
10-day	n.s.	n.s.	n.s.
14-day	n.s.	n.s.	n.s.
21-day	n.s.	n.s.	n.s.
28-day	n.s.	n.s.	n.s.
		Mixed	
5-day	n.s.	n.s.	n.s.
10-day	n.s.	n.s.	n.s.
14-day	n.s.	n.s.	n.s.
21-day	n.s.	n.s.	n.s.
28-day	n.s.	n.s.	n.s.

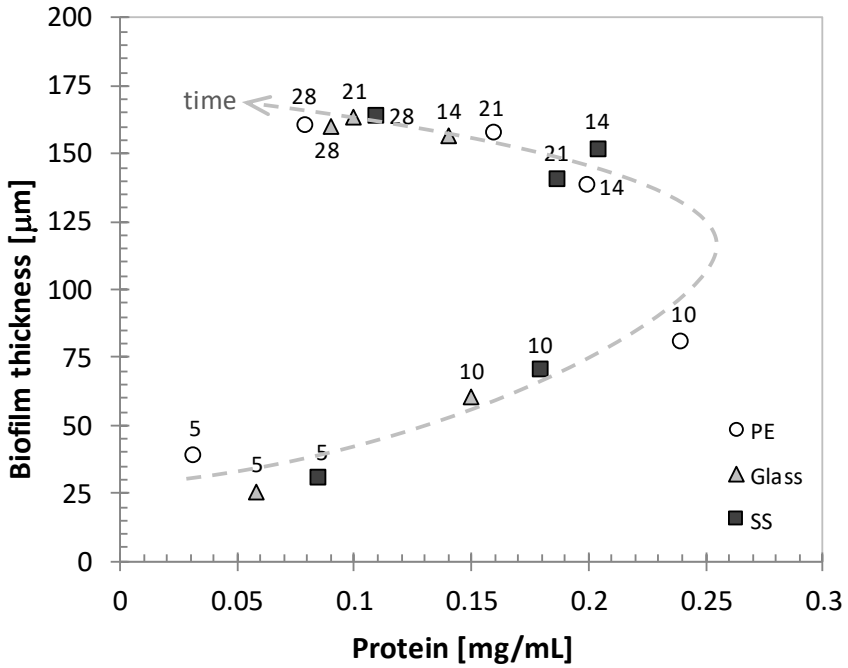

(a)

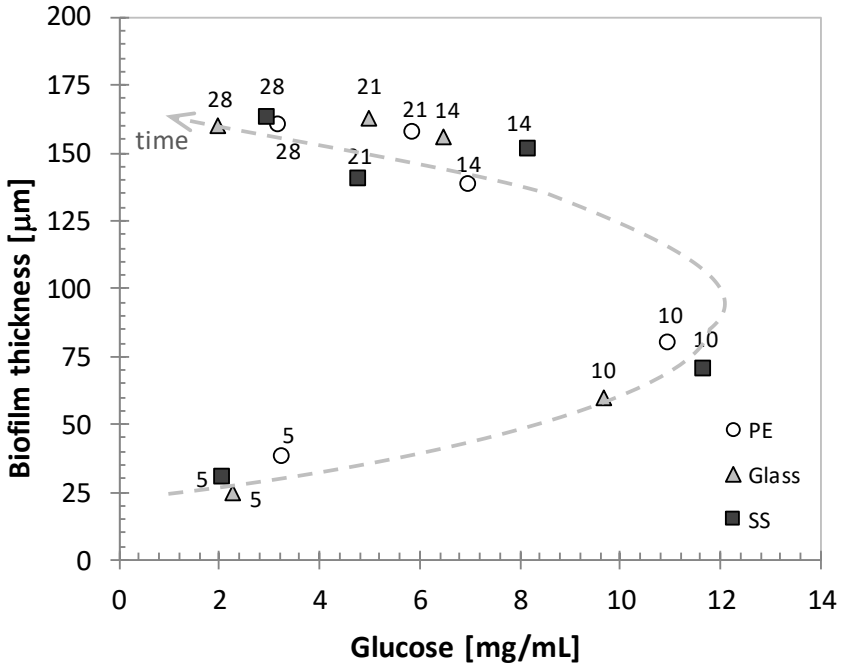

(b)

Figure 5: Comparisons between biofilm thickness and amounts of (a) protein and (b) glucose in *E. coli* biofilms. The labels show the incubation periods (in days).

3.4 Biofilm strength

The results for destructive strength testing for all 10-day and 10*-day *E. coli* biofilms are shown in Figure 6, in which the percentage of average thickness is plotted against the applied gauging shear stress estimated from equation (1). Error bars have been omitted to avoid over-crowding of the figure. There appears to be two distinct stages in the removal process for both 10-day and 10*-day biofilms. Shear stress values of approximately 6 Pa and 15 Pa are required to reduce the thickness to 30-35% of the original thickness for 10-day and 10*-day biofilms, respectively. Following this stage, however, a significant increase in shear stress to more than 15 Pa and 30 Pa is required to remove the remaining layers which are closer to the substrate. This is reasonable because the top layer of the biofilm, which mainly consists of loosely attached cells and fresh EPS, is more susceptible to shear induced removal. All biofilms exhibited a similar removal behaviour. The results also show that the type of substrate has minimal effects on the removal behaviour. Although the effect of desiccation had an insignificant effect upon the biofilm thickness (Figure 4(a)), the adhesive (biofilm-substrate) and cohesive (biofilm-biofilm) strengths almost doubled. This confirms that an interruption to a biofilm development process may cause an undesired impact (e.g. an accelerated attachment process) which affects biofilm growth and it is possible that a desiccated biofilm may produce an additional evaporation barrier and denser EPS, which may result in a stronger biofilm (Flemming *et al.* 2016). The starvation of cells usually results in them developing additional EPS layers, subsequently making them stronger, and harder to disrupt with disinfectants.

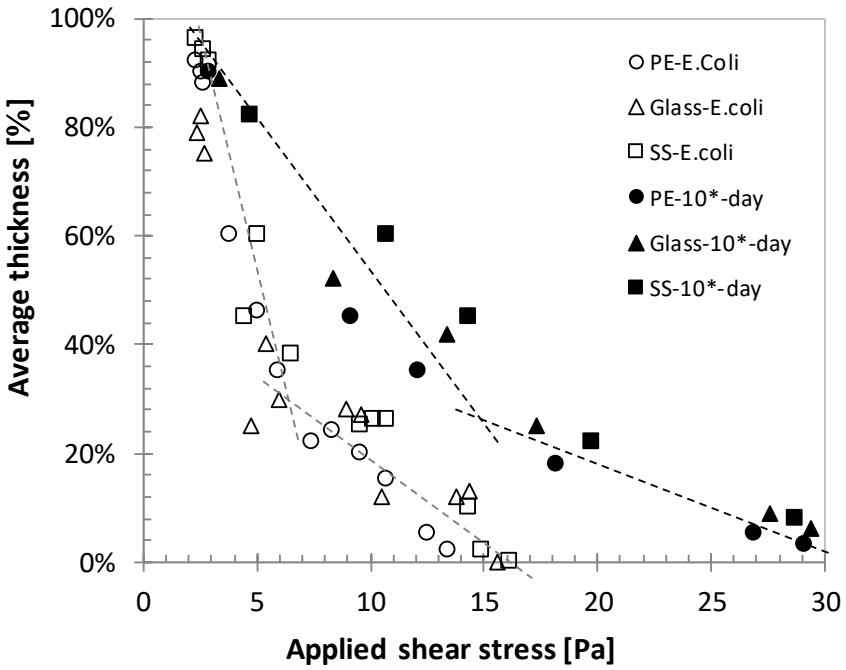

Figure 6: The strength testing results for all 10-day and 10*-day *E. coli* biofilms. The dashed lines are drawn to aid visualisation.

Figure 7 shows that the adhesive strength of mixed biofilms grown on the three substrates increased rapidly between 5 and 14 days. This behaviour suggests that the biofilms developed its strength substantially during that period. The strength of the biofilms showed a significant decline after 21 and 28 days. This means that the biofilms grown for 5 and 21-28 days were the easiest to remove, whilst those grown for 10 and 14 days proved to be more resilient. The adhesive strength of the biofilms (95% removal) appears to be strongly correlated to the protein content, as shown in Figure 8(a). The correlation between glucose content and adhesive strength is less clear especially for 10-day and 14-day biofilms, as shown in Figure 8(b). This suggests that the levels of protein in the biofilm are more of a factor in biofilm strength than glucose, particularly in establishing strong bonds with the surface. Flemming and Wingender (2010) reported that protein and polyssaccharide in EPS enable the initial steps in the colonisation of surfaces by planktonic cells, and the long-term attachment of whole biofilms to surfaces. They also enable bridging between cells, the temporary immobilisation of bacterial populations, the development of high cell densities and cell–cell

recognition. The strength profiles for *E. coli* biofilms (results not shown) are similar to those shown in Figure 6, whereby the adhesive strength peaked at 14 days. The biofilms become weaker at 21 days and this is supported by the CLSM images in Figures 9(a) and (b) which clearly shows the increase percentage of dead cells (red) from approximately 38% ± 8% to 86% ± 2% for 14 days and 21 days, respectively. It is also noteworthy that although the strength of biofilms peaked at 14 days, there is a reasonable presence of dead cells. The strength and thickness values obtained in these experiments are similar in order of magnitude to those reported by Peck *et al.* (2015) where mono-culture *E. coli* biofilms were generated under static *i.e.* no bulk flow conditions, since the Reynolds number employed in this study is low i.e. $Re \sim 15$. It is interesting to note that the strength values of *Pseudomonas aeruginosa* PAO1 grown under turbulent flow conditions (Suwarno *et al.*, 2017) obtained using FDG were two orders of magnitude larger. This confirms the mechanical properties of biofilms can be influenced by shear forces suggesting that biofilms can undergo phenotypic adaptation.

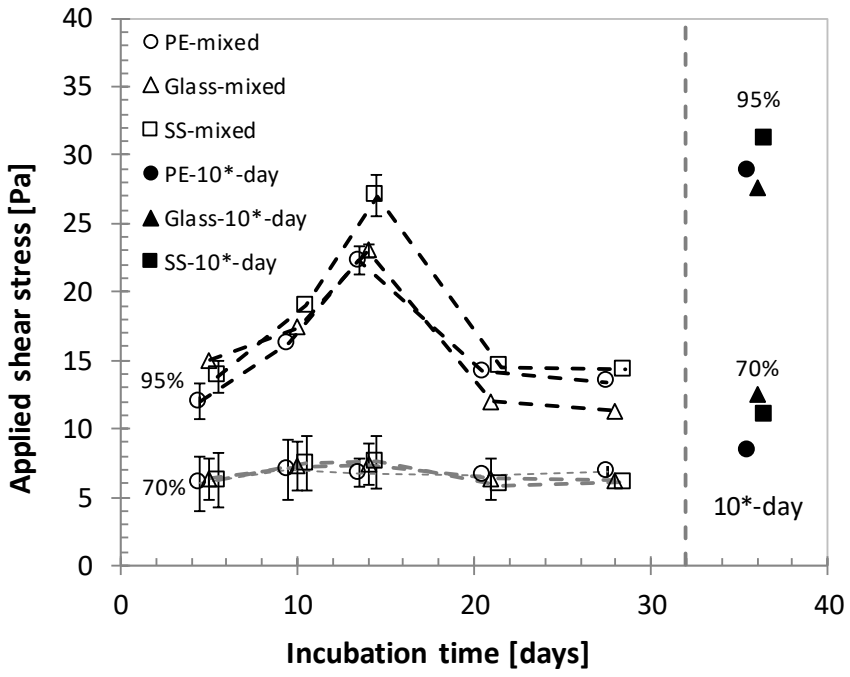

Figure 7: The applied shear stress required to remove 70% and 95% thickness of mixed biofilms.

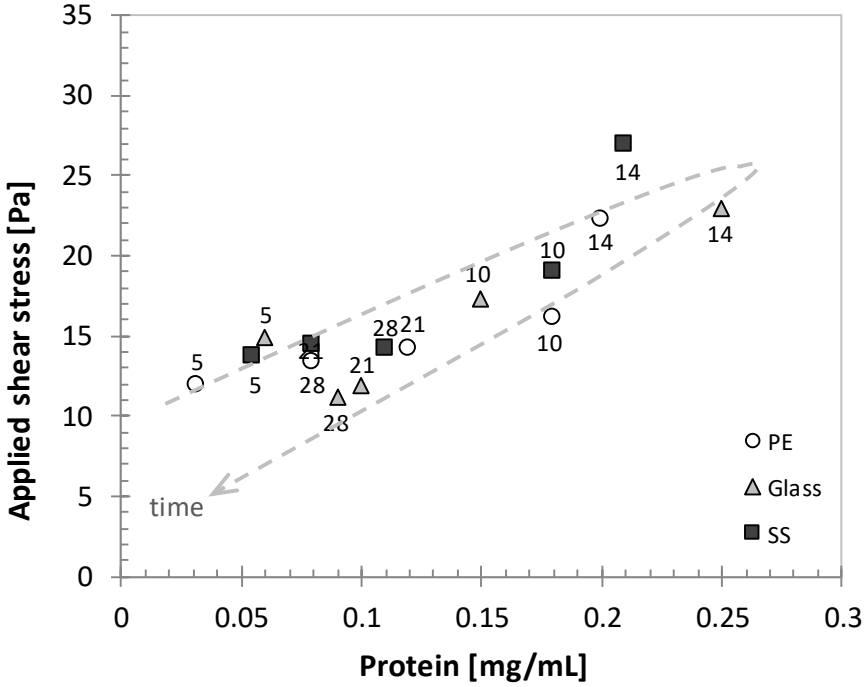

(a)

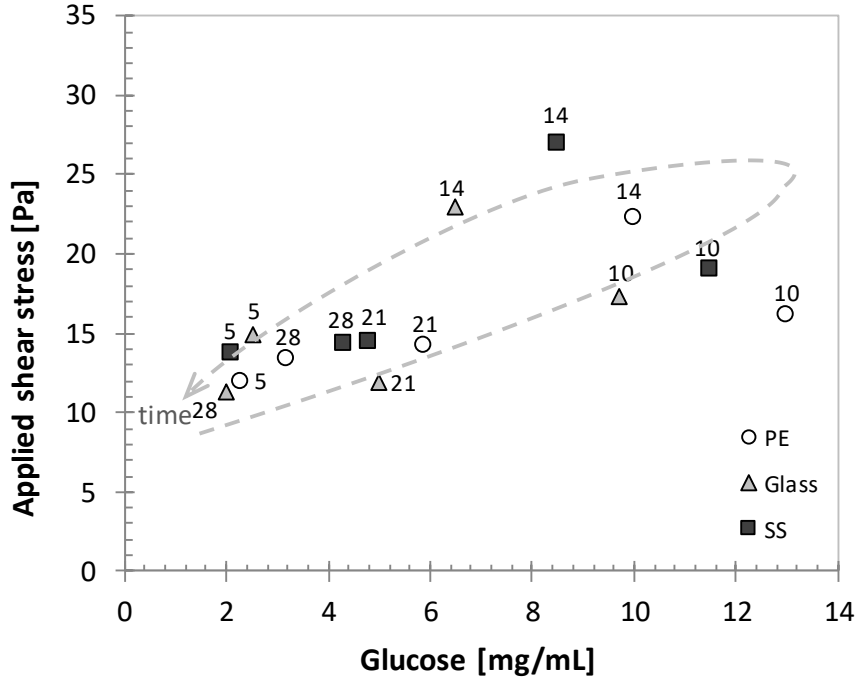

(b)

Figure 8: Comparisons between mixed biofilm strength (95% removal) and amounts of (a) protein and (b) glucose in mixed biofilms. The labels show the incubation periods (in days).

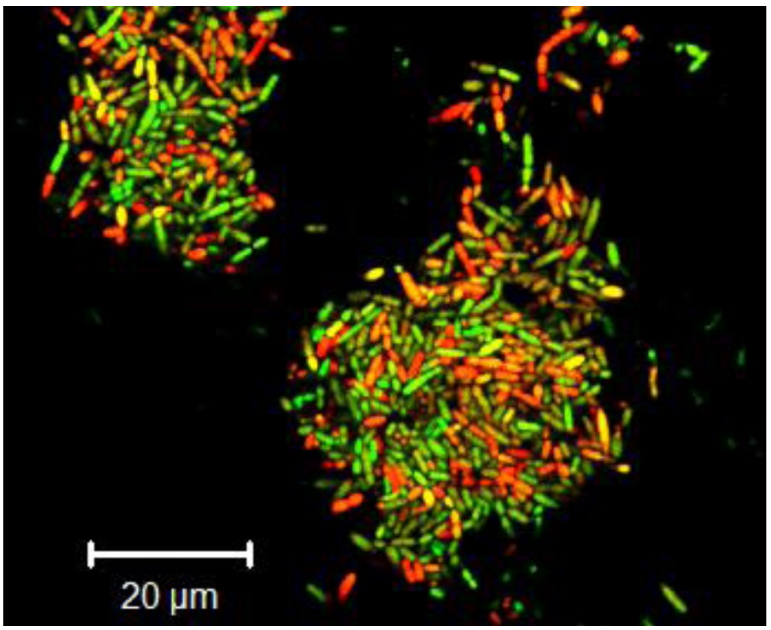

(a)

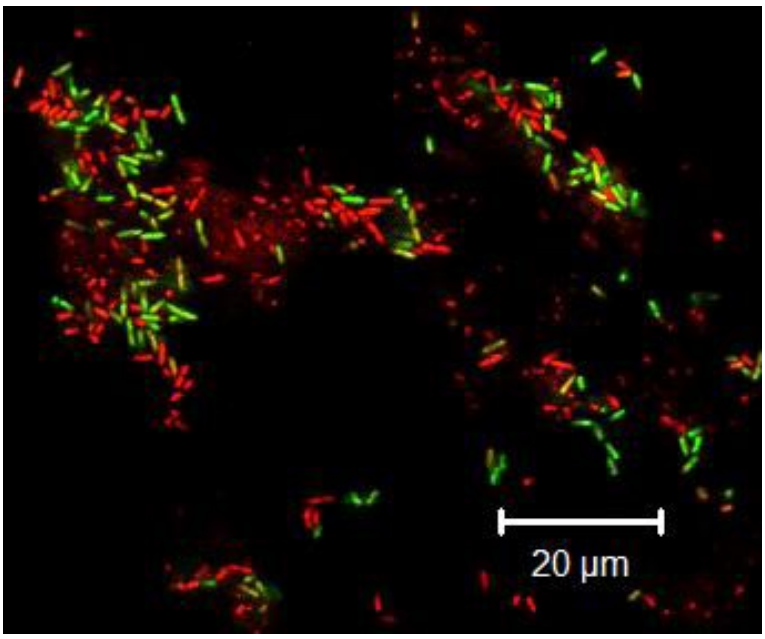

(b)

Figure 9: CLSM images showing the presence of live and dead cells in *E. coli* biofilms grown on glass for (a) 14 days; and (b) 21 days. Live cells are stained green, dead cells are stained red.

Analysis using the FDG and CLSM techniques provided unique additional information related to biofilm strength and thickness and how do these parameters correlate with protein and glucose

content in EPS through an on-line and simple method. These information is essential to provide informed guidance to cleaning scheduling and can be correlated to the requirements of foulant removal energy. The results in this study will also provide an avenue for more developments on the use of FDG in future studies related to biofouling.

Conclusions

The aim of this work was to investigate the development and removal of *E. coli* and *B. cepacia* biofilms from a range of substrates by using fluid dynamic gauging (FDG). FDG has been used successfully to determine the yield strength of biofilm adhesion and the strength of intercellular cohesion within biofilms, as a function of incubation time. The results indicate a relationship between maturity and biofilm strength, with a peak after a growth period of 14 days, with weakened structures evident as the biofilms age further. This suggests that less energy would be required to remove biofilms in either the period between establishment and 5 days growth, or after more than 21 days growth rather than in the period in between. However, in developing any biofilm treatment protocol, the relevant costs and risks of product contamination would need to be taken into account, and adjustments made accordingly. The interruption of the flow of media during biofilm development also increased the biofilm strength significantly, and this should be avoided in industrial operational situations wherever possible.

Nomenclature

d	Diameter of tube [m]
d_t	Diameter of nozzle throat [m]
h	Clearance between nozzle and biofilm [m]
h_o	Clearance between nozzle and substrate [m]
m_g	Mass flow rate [kg s^{-1}]
Re	Reynolds number [-]

w	Width of nozzle rim [m]
μ	Dynamic viscosity [Pa s]
ρ	Density [kg m^{-3}]
τ_w	Shear stress [Pa]

Acronyms

AFM	Atomic force microscopy
CLSM	confocal laser scanning microscopy
EPS	extracellular polymeric substances
FDG	fluid dynamic gauging
PBS	phosphate-buffered saline
SWR	standard working reagent

Acknowledgements

O.P.W. Peck would like to thank the University of Bath for the University Research Studentship. The authors would like to thank Kate Meredith (Department of Pharmacy and Pharmacology) for technical support in biofilm growth. *E. coli* and *B. cepacia* were kindly provided by Dr Harold Tjalsma of the Radboud University Nijmegen Medical Centre. We would also like to thank Dr Alistair Muir and Mr Fernando Acosta (Department of Chemical Engineering) for their assistance with the optical microscope and Dr Adrian Rogers for his expertise in the use of the confocal laser scanning microscope.

References

Alsteens D., Etienne D., Paul G. R., Alain R. B., Yves F. D. (2007) Direct Measurement of Hydrophobic Forces on Cell Surfaces Using AFM. *Langmuir*: *The ACS Journal of Surfaces and Colloids*, **23**(24), 11977–79.

Blanchard A.P., Bird M.R., Wright S.J.L. (1998) Peroxygen disinfection of *Pseudomonas aeruginosa* biofilms on stainless steel discs. *Biofouling*. **13**, 233-253.

Bos R., H. C. van der Mei, Gold J., Busscher H. J. (2000) Retention of bacteria on a substratum surface with micro-patterned hydrophobicity. *FEMS Microbiology Letters*, **189**(2), 311–315

Buc, S. S., Farhat N., Kruithof J. C., Picioreanu C., van Loosdrecht M. C. M., Vrouwenvelder J. S. (2018) Review on strategies for biofouling mitigation in spiral wound membrane systems. *Desalination*, **434**, 189-197.

Burton, Z. F., and Kaguni, J. M., *Experiments in Molecular Biology: Biochemical Applications*, pp. 22-25, Academic Press, San Diego, 1997.

Carpentier B, Cerf O. (1993) Biofilm and their consequences with particular reference to hygiene in the food industry. *J. Appl. Bacteriol.*, **75**, 499-511.

Chen X., Suwarno S. R., Chong T. H., McDougald D., Kjelleberg S., Cohen Y., Fane A. G., Rice S. A. (2013) Dynamics of biofilm formation under different nutrient levels and the effect on biofouling of a reverse osmosis membrane system. *Biofouling*, **29**, 319-330.

Chew Y.M.J., Paterson W.R., Wilson D.I. (2004). Fluid dynamic gauging for measuring the strength of soft deposits. *J Food Eng.*, **65**, 175-187.

Choi YC, Morgenroth E. (2003) Monitoring biofilm detachment under dynamic changes in shear stress using laser-based particle size analysis and mass fractionation. *Water Sci. Technol.*, **47**, 69-76.

De Kievit T.R., Gillis R., Marx S., Brown C., Iglewski B.H. (2001) Quorum-Sensing Genes in Pseudomonas Aeruginosa Biofilms: Their Role and Expression Patterns. *Appl. Environ. Microbiol.*, **67**(4), 1865–73.

Dreszer C., Vrouwenvelder J.S., Paulitsch-Fuchs A.H., Zwijnenburg A., Kruithof J.C., Flemming H.-C. (2013) Hydraulic Resistance of Biofilms. *J. Memb. Sci.*, **429**, 426-447.

DuBois M., Gilles K.A., Hamilton J.K., Rebers P.A., Smith F. (1956) Colorimetric Method for Determination of Sugars and Related Substances. *Anal. Chem.*, **28**, 350-356.

Finlay J. A., Maureen E. C., Linnea K. I., Gabriel P. L., James A. C. (2002) The influence of surface wettability on the adhesion strength of settled spores of the green alga enteromorpha and the diatom amphora. *Integrative and Comparative Biology*, 42(6), 1116-1122.

Flemming H-C., Wingender J. (2010) The biofilm matrix. *Nature Reviews: Microbiology*, **8**, 623-633.

Flemming H-C., Wingender J., Szewzyk U. 2011. Biofilm Highlights. Berlin Heidelberg: Springer-Verlag.

Flemming H-C., Wingender J., Szewzyk U., Steinberg P., Rice S.A., Kjelleberg S. (2016) Biofilms: an emergent form of bacterial life. *Nat. Rev. Microbiol.*, **14**, 563–575.

Garnett J. A., Matthews S. (2018) Interactions in Bacterial Biofilm Development: A Structural Perspective. *Curr. Protein and Pept. Sci.*, **13**(8), 739-755.

Gilbert P., Evans D. J., Evans E., Duguid I. G., Brown M. R. W. (1991) Surface characteristics and adhesion of *Escherichia coli* and *Staphylococcus epidermidis*. *J. Appl. Bacteriol.*, **71**, 72-77.

Gule N. P., Begum N. M., Klumperman B. (2016) Advances in biofouling mitigation: A review. *Crit. Rev. Environ. Sci. Technol.*, **46**(6), 535-555.

Jamaly S., Darwish N. N., Ahmed I., Hasan S. W. (2014) A short review on reverse osmosis pretreatment technologies. *Desalination*, **354**, 30-38.

Kögler M., Zhang B., Cui L., Shi Y., Yliperttula M., Laaksonen T., Viitala T., Zhang K. (2016) Real-time Raman based approach for identification of biofouling. *Sens Actuators B Chem.*, **230**, 411-421.

Makovcova J.,Babak V., Kulich P., Masek J., Slany M., Cincarova L. (2017) Dynamics of mono- and dual-species biofilm formation and interactions between *Staphylococcus aureus* and Gram-negative bacteria. *Microb. Biotechnol.*, **10**(4), 819-832.

Mascotti, K., McCullough J., Burger S. R. (2000) HPC Viability Measurement: Trypan Blue versus Acridine Orange and Propidium Iodide. *Transfusion*, **40**(6), 693-696.

Momba M.N.B., Kfir R., Venter S.N., CLeote T.E. (2000) An overview of biofilm formation in distribution systems and its impact on the deterioration of water quality. *Water SA*., **26**, 59-66.

Mukherjee M., Menon N. V., Liu X., Kang Y., Cao B. (2016) Confocal laser scanning microscopy-compatible microfluidic membrane flow cell as a nondestructive tool for studying biofouling dynamics on forward osmosis membranes. *Environ. Sci. Technol. Lett.*, **3**, 303–309

Paul E., Ochoa J.C., Pechaud Y., Liu Y., Liné A. (2012) Effect of shear stress and growth conditions on detachment and physical properties of biofilms. *Water Res.*, **46**, 5499-5508.

Peck O. P. W. (2017) *An investigation into the strength and thickness of biofouling deposits to optimise chemical, water and energy use in industrial process cleaning*. PhD Dissertation, University of Bath, UK.

Peck O. P. W., Chew Y. M. J., Bird M. R., Bolhuis A. (2015) Application of fluid dynamic gauging in the characterization and removal of biofouling deposits. *Heat Transfer Engineering*, **36**(7-8), 685-694.

Powell L. C., Hilal N., Wright C. J. (2017) Atomic force microscopy study of the biofouling and mechanical properties of virgin and industrially fouled reverse osmosis membranes. *Desalination*, **404**, 313-321.

Rose H., Baldwin A., Dowson, C. G., Mahenthiralingam, E. (2009) biocide susceptibility of the burkholderia cepacia complex. *J. Antimicrob. Chemother.*, **63**(3), 502-10.

Schleheck D., Nicolas B., Janosch K., Jeremy S. W., Diane McD., Scott A. R., and Staffan K. (2009) Pseudomonas aeruginosa PAO1 preferentially grows as aggregates in liquid batch cultures and disperses upon starvation. *PLoS ONE*, **4**(5), e5513.

Schumann P., Pukall R. (2013) The discriminatory power of ribotyping as automatable technique for differentiation of bacteria. *Syst. Appl. Microbiol*., **36**(6), 369-375.

Sim S. T. V., Suwarno S. R., Chong T. H., Krantz W. B., Fane A. G. (2013) Monitoring membrane biofouling via ultrasonic timedomain reflectometry enhanced by silica dosing. *J. Membr. Sci.*, **428**, 24–37.

Smith P.K., Krohn R.I., Hermanson G.T., Mallia A.K., Gartner F.H., Provenzano M.D., Fujimoto E.K., Goeke N.M., Olson B.J., Klenk D.C. (1985) Measurement of protein using bicinchoninic acid. *Anal. Biochem.*, **150**, 76–85.

Srey S., Jahid I. K., Ha S-D. (2013) Biofilm formation in food industries: A food safety concern. *Food Control*, **31**, 572-585.

Suwarno S.R., Huang W., Chew Y.M.J., Tan S.H.H., Trisno A.E., Zhou Y. (2017) On-line biofilm strength detection in cross-flow membrane filtration systems. *Biofouling*, **34**, 123-131.

Wang, C., Lan C. Q. (2018) Effects of shear stress on microalgae – A review. *Biotech. Adv.*, **36**, 986-1002.

Whitehead K. A., Verran J. (2015) Formation, architecture and functionality of microbial biofilms in the food industry. *Current Opinion in Food Science*, **2**, 84-91.

Wimpenny J. W. T., Kinniment S. L., Scourfield M. A. (1993) The physiology and biochemistry of biofilm. In *Microbial Biofilms: Formation and Control* ed. Denyer S. P., Gorman S. P. and Sussmann M. Oxford: blackwell Scientific Publications.

Wingender J., Neu T.R., Flemming H-C. (1999) Microbial Extracellular Polymeric Substances. Duisburg Magdeburg: Springer-Verlag.

Yebra D.M., Kiil S., Weinell C.E., Dam-Johansen K. (2006) Effects of marine microbial biofilms on the biocide release rate from antifouling paints—A model-based analysis. *Prog. Org. Coat.*, **57**, 56-66.